Structural and electronic properties of Y-based metallic glasses

1992 J. Phys.: Condens. Matter 4 9557

(http://iopscience.iop.org/0953-8984/4/48/011)

J. Phys.: Condens. Matter 4 (1992) 9557–9572. Printed in the UK

Structural and electronic properties of Y-based metallic glasses

Ch Hausleitner†, M Tegze†‡ and J Hafner†

† Institut für Theoretische Physik, TU Wien, Wiedner Hauptstraße 8–10, A-1040 Wien, Austria

‡ Central Research Institute for Physics, PO Box 49, H-1525 Budapest, Hungary

Received 10 February 1992, in final form 5 June 1992

Abstract. Calculations of the atomic structure and the electronic spectrum of Y-based transition-metal glasses are presented. Our investigations are based on a hybridized nearly-free-electron tight-binding-bond approach to the interatomic forces, a molecular-dynamics modelling of the atomic structure, and linear-muffin-tin-orbital supercell calculations of the electronic density of states and of the photoemission intensities. Our results explain the physical origin of the strong chemical and topological short-range-order effects observed in these materials and their relation to the d-band shifts observed in the photoelectron spectra.

1. Introduction

Metallic glasses formed by two transition elements have been the focus of intense research efforts during the past decade. The interest in these systems is generated by their many interesting properties.

(a) Metallic glasses are formed by many different combinations of transition elements, ranging from near neighbours in the periodic table to combinations with a large difference in the number of d valence electrons in the constituents, and often over a wide range of compositions [1];

(b) X-ray and neutron-diffraction experiments have shown that these glasses possess a high degree of chemical and topological short-range order (SRO) [2–4]. There are clear indications that the SRO increases with an increasing difference in the number of d electrons of the constituent metals;

(c) Photoemission studies [5–11] have demonstrated that the alloy spectrum cannot be obtained by a superposition of the pure elements: the valence band of the *late* transition metal (i.e. the one with the higher number of d electrons) is shifted to larger binding energies. From this we can conclude that transition-metal glasses are strongly interacting systems to which no simple picture such as a rigid-band model can be applied. According to all evidence the degree of short-range order found in the atomic structure scales with the covalent binding effects observed in photoemission;

(d) Many transition-metal glasses are superconducting [12,13], the Fe- and Co-rich glasses are magnetically ordered with a rich variety of spin structures ranging from inhomogeneous ferro- and ferrimagnetism to asperomagnetism and spin-glass behaviour [14–17].

0953-8984/92/489557+16$07.50

Today, a wealth of experimental data on these systems are available, but we have to admit that theoreticians have been unable to keep abreast of the advance in experimental research. The reason is that any theoretical calculation of material properties has to be based on a sufficiently realistic structural model of the glass structure. The modelling of glasses in turn requires the availability of accurate interatomic forces as an input to the simulation algorithm. It is precisely the high degree of covalency in the transition-metal bond that makes a calculation of interatomic forces in transition-metal systems so difficult.

Recently, a certain breakthrough in this field has been achieved through the revival of an old concept: the bond order [18]. The interaction between a pair of atoms i, j may be expressed in terms of the transfer integral $t(R_{ij})$ and the bond order Θ_{ij} defined as the difference in the number of electrons in bonding and antibonding linear combinations of the tight-binding orbitals centred at sites i and j. At least formally, the product of the transfer integral and the bond order defines a pair interaction $\Phi_{ij} \propto t(R_{ij})\Theta_{ij}$. However, the bond order depends on the atomic environment so that in general Φ_{ij} is not an isotropic pair interaction. Over the last few years it has become clear that an accurate description of interatomic forces in the *early* BCC transition metals necessitates the inclusion of angular terms. Tight-binding techniques for the calculation of these many-body forces have been derived in the form of cluster expansion [19–21] (based on a linearization of the moment–recursion coefficient relations) and moment expansions [22, 23]. These results show very clearly that the importance of the many-body interactions depends largely on the higher moments, i.e. on the structure of the electronic density of states. In a disordered (liquid or amorphous) alloy, the structure in the density of states is largely smeared out. Hence it should be possible to obtain a much more rapid convergence of the many-body expansion.

Very recently we have presented a new bond-order approach to interatomic forces in transition metals [24–26]. In our method we replace the actual atomic environment by a disordered Bethe lattice. This allows for an analytic calculation of the bond order and leads to an expression for the interatomic forces in terms of isotropic, albeit strongly non-additive pair forces. Our approach is in the spirit of the embedded-atom method [27] in that it attempts to absorb the complex many-body interactions in the bond order. It has been shown that the nature of the effective pair interaction depends strongly on the structure of the d band: a large difference in the d-state occupancy of the components leads to a valence band close to the split-band limit, the strong interaction in the d band is reflected in strongly non-additive pair interactions with a preference for unlike-atom bonds that are considerably shorter than the average of the like-atom bonds.

We have tested our approach in a series of modelling studies for Ni-based metallic glasses and found excellent agreement with experiment [24–26]. The new structural models have been used as the basis for self-consistent electronic structure calculations for Ni–Zr glasses [28], and for spin-polarized calculations of the electronic and magnetic structure of Fe–, Co–, and Ni–Zr glasses [29, 30].

In this paper we present the results of a systematic investigation of the structural and electronic properties of amorphous alloys of Y with Mn, Fe, Ni, Cu, and Zn. Our aim is to study the variation of chemical and topological short-range order and their relation to the changes in the structure of the valence band as a function of the relative position of the elements in the periodic table.

Our paper is organized as follows: in section 2 we present the interatomic forces derived from our hybridized nearly-free-electron tight-binding-bond approach, in section 3 we summarize the results of our molecular-dynamics simulations for the atomic struc-

ture. Section 4 contains the electronic DOS calculated using our self-consistent linear-muffin-tin-orbital supercell approach, and the calculated photoemission intensities. Our conclusions are presented in section 5.

2. Interatomic forces

The basic assumption is that the total energy can be written in the form

$$E = E_s + E_d = E_0(\Omega) + \frac{1}{2N_a}\sum_{\substack{i,j \\ i\neq j}} \Phi_s(\Omega; R_{ij}) + \frac{1}{2N_a}\sum_{\substack{i,j \\ i\neq j}} \Phi_{d-rep}(R_{ij}) + E_{d-bond}. \tag{1}$$

The s-electron contribution is treated in standard pseudopotential theory [31,32]. It contributes a volume energy E_0 and a set of density-dependent pair forces $\Phi_s(\Omega; R)$. We use the simple empty-core form of the pseudopotential [33] and the Ichimaru–Utsumi [34] local-field correction to the dielectric function of the electron gas.

The d-electron contribution may be written within the local-density approximation [20,35] in terms of a repulsive pair interaction containing the electrostatic, exchange-correlation and non-orthogonality contributions to the total energy and a covalent bond energy E_{d-bond} resulting from the formation of a d-electron band with the local density of states $n_{d,i}(E)$

$$E_{d-bond} = \sum_i \int^{E_F} (E - E_{d,i}) n_{d,i}(E)\, dE = E_{d-band} - \sum_i N_{d,i} E_{d,i}. \tag{2}$$

s–d hybridization is taken into account in an approximate way by setting the numbers N_s and N_d of s and d electrons equal to the values resulting from a self-consistent bandstructure calculation for the pure crystalline metals [36,37].

Assuming the d orbitals in the amorphous metals to be degenerate and neglecting the directionality of the d–d bond (which seems to be a legitimate first approximation in a glassy system), E_{d-bond} can be written in a two-centre orthogonal tight-binding approximation as

$$E_{d-bond} = \frac{1}{2N}\sum_{\substack{i,j \\ i\neq j}} t_{ij}(R_{ij})\Theta_{ij} \tag{3}$$

where t_{ij} is the transfer integral and the bond order Θ_{ij} counts the difference in the number of electrons in the bonding $|\phi^+\rangle = (1/\sqrt{2})(|\varphi_i\rangle + |\varphi_j\rangle)$ and in the antibonding states $|\phi^-\rangle = (1/\sqrt{2})(|\varphi_i\rangle - |\varphi_j\rangle)$ (the indices i and j stand for the atomic sites as well as the orbital). It may be shown that the bond order is given by the integral over the imaginary part of the off-diagonal Green's function,

$$\Theta_{ij} = -\frac{2}{\pi}\int^{E_F} \mathrm{Im}\, G_{ij}(E)\, dE. \tag{4}$$

Θ_{ij} has to be calculated for an appropiately chosen reference system. In [24–26] we have developed a transfer-matrix method for the analytic calculation of the bond order on a random Bethe lattice. In the Bethe lattice reference system, the bond order

depends on the local atomic environment only via the coordination number Z and the chemical order. We have chosen $Z = 12$, corresponding to the close-packed crystalline and liquid [37] metals. In amorphous alloys, the actual coordination number may be slightly higher, but for high values of Z ($Z \geqslant 9$) the coordination-number dependence of the pair interactions is very weak [37]. The choice of a random reference system is in the spirit of the local-force theorem [38–40] and leads to very accurate ordering potentials [27]. In a binary alloy we have to solve the problem of charge self-consistency. One possibility is to shift the on-site energies $E^{\alpha}_{d,i}$ (α labels the chemical species) such that there is no change in the orbital occupancy relative to the pure-metal reference value [19,20]. The local-force theorem of density functional theory [38–40] may be used to show that the change in the *bond* energy under this constraint is to first order equal to the change in the *band* energy at fixed on-site energies. The consequence is that changes in the electrostatic and double-counting contributions to the total energy compensate each other. Hence the decomposition of the total energy into pairwise repulsive and bonding contributions remains valid.

The calculation of the effective interatomic potentials proceeds as follows

(i) The d-electron on-site energies $E^{\alpha}_{d,i}$ are calculated for the configuration s^1d^{N-1} of the free atom.

(ii) The average transfer integrals $t^{\alpha\beta}_{ij}$ for nearest-neighbour d–d interactions are calculated in a second-moment approximation and fitted to the canonical band-widths of Andersen and Jepsen [41].

(iii) The numbers N^{α}_{s} and N^{α}_{d} of s and d electrons for each component are taken from a self-consistent bandstructure calculation of the pure metals [36].

(iv) The s-electron pseudopotential radius R_c is determined by fitting the structure of the pure liquid metal [37].

Table 1. Input parameters for the calculation of the interatomic forces: atomic volume Ω, nearest-neighbour distance in the crystal d, number of s electrons N_s, number of d electrons N_d, d electron energy level E_d, d-band width W_d, and s electron pseudopotential radius R_c.

	Y	Mn	Fe	Ni	Cu	Zn
Ω (Å^3)	35.75	12.22	11.78	10.94	11.81	15.12
d (Å)	3.56	2.52	2.48	2.49	2.55	2.66
N_s	1.31	1.43	1.42	1.40	1.44	2.20
N_d	1.69	5.57	6.58	8.60	9.56	9.80
E_d (eV)	− 2.94	− 5.09	− 5.57	− 6.48	− 6.92	−13.97
W_d (eV)	6.59	5.60	4.81	3.78	2.80	1.30
R_c (Å)	1.30	0.87	0.80	0.58	0.48	0.55

Numerical values of all parameters for the metals involved in this study are given in table 1. Note that all parameters are determined for the pure metals, no new parameters are introduced for describing the alloys. For any details of our method we refer to [26].

Figure 1 shows the Bethe lattice densities of states (DOS) for $Fe_{35}Y_{65}$ and $Cu_{35}Y_{65}$, together with the imaginary part of the off-diagonal Green's function. The Y–Fe system shows largely overlapping Fe d and Y d DOSs forming together a nearly rectangular band. The Fermi level falls close to the zero in Im $G_{YFe}(E)$, so that the Y–Fe bond order is close to the maximum value possible in this system (table 2). This results in a strong preference for the Y–Fe nearest-neighbour pairs in the interatomic potential (see

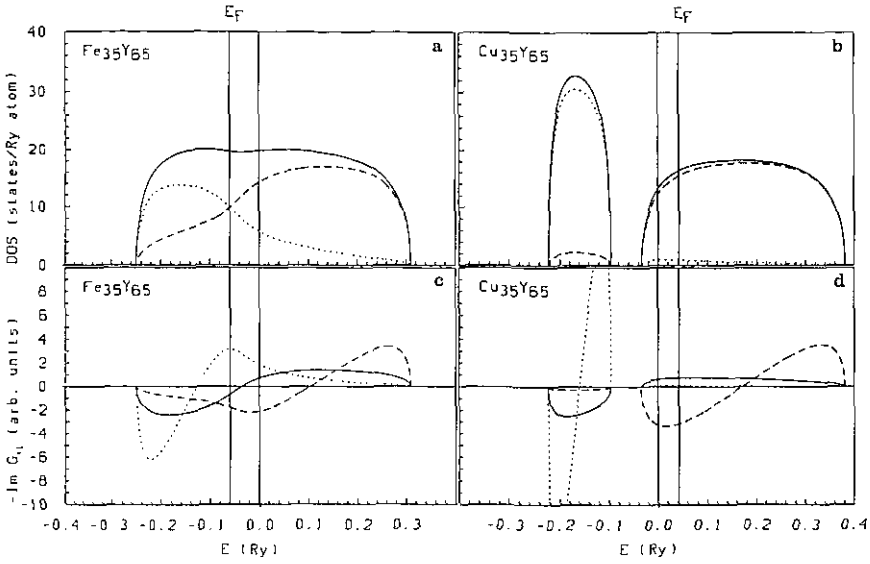

Figure 1. (a), (b) Total and site-decomposed electronic DOS of Y–Fe and Y–Cu alloys on a random Bethe lattice. Dashed line—partial Y DOS, dotted line—partial Fe (Cu) DOS, full line—total DOS. (c), (d) Imaginary part of the off-diagonal Green's functions Im $G_{ij}(E)$: dashed line—G_{Y-Y}, dotted line—G_{Fe-Fe} (G_{Cu-Cu}), full line—G_{Y-Fe} (G_{Y-Cu}).

figure 2). Y–Cu on the other hand is a split-band alloy, with only weak hybridization of the Cu and Y d bands. The weak hybridization results in a rather small amplitude of the Y–Cu Green's function, and hence a smaller bond-order (table 2). The Y–Y bond-order is large in all alloys, it increases from Y–Mn to Y–Cu because of a reduced bonding–antibonding mixing in the lower part of the Y d band. The bond-order of the late transition metal decreases drastically in the same sequence because with increasing band-filling, more antibonding states are populated.

Table 2. Bond-order Θ_{ij} for covalent d–d interactions in $Y_{65}X_{35}$ alloys calculated on a random Bethe lattice.

Alloy	Θ_{Y-Y}	Θ_{Y-X}	Θ_{X-X}
$Y_{65}Mn_{35}$	−1.089	−2.275	−2.805
$Y_{65}Fe_{35}$	−1.211	−2.307	−2.189
$Y_{65}Ni_{35}$	−1.382	−2.036	−0.605
$Y_{65}Cu_{35}$	−1.606	−1.300	−0.0923
$Y_{65}Zn_{35}$	−1.693	−0.884	−0.0029

A remarkable feature of all potentials is that the first minimum of the Y–X potential (X = Mn, Fe, Ni, Cu, Zn) occurs at a distance that is shorter than the average distance of the minima of the Y–Y and X–X potentials. This non-additivity increases with increasing difference in the number of d electrons (i.e. in the sequence X = Mn, Fe, Co, Ni), but it decreases again once the d band of the second metal is completely filled (X = Cu, Zn).

A similar trend is found in the strength of the attractive interactions. In the series Y–Mn, Y–Fe, Y–Ni there is an increasing preference for the formation of Y–X nearest-neighbour pairs due to a strong covalent interaction between unlike atoms. Once the d

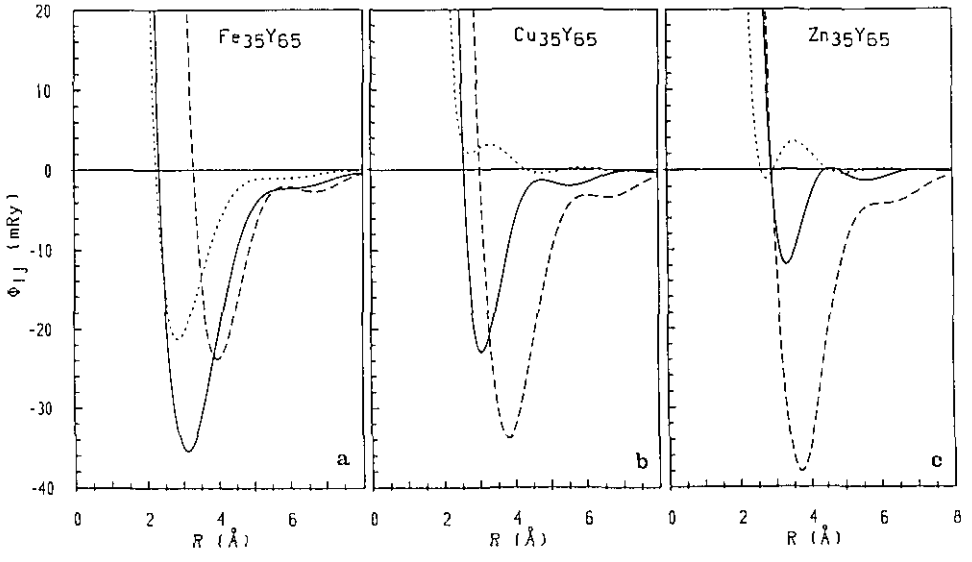

Figure 2. (a)–(c): Effective interatomic potentials $\Phi_{i,j}(R)$ for $Y_{65}X_{35}$ alloys, X = Fe, Cu, Zn. Dashed line—Φ_{Y-Y}, dotted line—Φ_{X-X}, full line—Φ_{Y-X}.

band of X has been completely (or nearly completely) filled, the strength of the covalent bond decreases again (see the Y–Cu potential in figure 2), and in Y–Zn like-atom bonds are preferred over unlike-atom bonds.

Altogether, we find a clear physical trend in the interatomic forces as a function of the difference in the number of d electrons ΔN_d whose origin can be traced back to the trend in the valence-band structure. With increasing ΔN_d the valence-band DOS changes from a common-band to a split-band form. This is due to an increase in the difference in the on-site energies $\Delta E = E_{d,Y} - E_{d,X}$ and a decrease in the bandwidth $W_{d,X}$ of the late transition metal X. In the common-band limit the bond orders for Y–Y, Y–X, and X–X pairs are of comparable order of magnitude. With the transition to the split-band regime the order of the X–X bonds decreases very rapidly, whereas the order of the Y–Y and Y–X bonds remains essentially constant. As a consequence we have $\Theta_{Y-X} \approx \frac{1}{2}(\Theta_{X-X} + \Theta_{Y-Y})$ in the common-band case and $\Theta_{Y-X} \geqslant \frac{1}{2}(\Theta_{X-X} + \Theta_{Y-Y})$ in the split-band case, expressing the non-additivity in the bonding d–d pair interactions. The repulsive d–d interactions on the other hand depend only on the overlap and transfer integrals and are independent of the form and the filling of the d band. The role of the s-electron contributions too is essentially to provide a repulsive potential to counterbalance the strong attractive d-electron forces. Consequently, the large bond order in unlike-atom bonds dominates the physical trends and leads to non-additive pair forces with a distinct preference for strong and short unlike-atom bonds.

3. Glass structure

3.1. Molecular-dynamics quenching

The pair potentials have been used to construct a model for the glass via a molecular-dynamics algorithm. The simulation is started in the liquid phase, at a temperature

several hundred degrees above the melting temperature. After reaching equilibrium, the liquid alloy was compressed isothermally to the density of the glass (where no experimental data for the density are available, Zen's law is assumed) and reequilibrated with the pair potentials recalculated for the density of the glass. Finally, the liquid is quenched to room temperature at constant volume. The simulations have been performed for two classes of ensembles with $N = 1372$ and $N = 64$ atoms respectively in a periodically repeated cubic box. For the large ensembles the interatomic potentials have been cut off at a distance corresponding to 30% of the edge of the MD cell, for the small ensembles the largest cut-off compatible with the minimum image convention was adopted. A fourth-order predictor–corrector algorithm with a time increment of $\Delta t = 10^{-15}$ s was used for the integration of the Newtonian equations of motion (for details see [42]), an efficient network-cube algorithm was used for nearest-neighbour book-keeping [43]. Typical runs allowed $\sim$ 3000 steps for equilibration and $\sim$ 2000 for production. The quenching rate was $dT/dt \simeq 10^{14}$ K s^{-1}.

The simulations for the large ensembles served to produce reliable correlation functions and static structure factors for comparison with experimental diffraction data. The small ensembles are used to create the atomic coordinates for the electronic structure calculation using a supercell approach. The configurations to be used in the supercell calculation were selected such that the correlation functions derived from a single 64-atom configuration are as close as possible to those calculated from an ensemble average for the large configurations.

3.2. Partial correlation functions

Figures 3(a)–(e) summarize the trends in the partial pair correlation functions. In amorphous Y–Mn and Y–Fe the local structure is dominated by the large size ratio ($R_Y/R_{Mn} = 1.43$, $R_Y/R_{Fe} = 1.45$) and by a tendency to form unlike-atom pairs. In addition, the Y–X bond-length is contracted slightly compared to the average of the Y–Y and X–X nearest-neighbour distances. Both the tendency to heterocoordination and the contraction of the Y–X bonds are even more pronounced in Y–Ni and Y–Cu glasses. In addition to a strong chemical short-range order (CSRO), these glasses are also characterized by a strong topological short-range order (TSRO) which manifests itself in the characteristic three-peak structure of g_{CuCu} and g_{NiNi}, and in the splitting of the second peak of g_{YY}. The trend to a SRO breaks down after the d band has been completely filled—the structure of the Y–Zn amorphous alloy is essentially a random close-packing of spheres with different diameters, with a slight trend to phase separation. These trends in the pair correlation functions clearly reflect the variations in the interatomic forces (see figure 2).

Of particular interest are the correlation functions of the smaller minority atoms only. Steeb *et al* [44] had already pointed out that there exists a surprising similarity between the bonds formed by B and P atoms in metal–metalloid (Ni–B, Fe–P, etc.) glasses and the bonds formed by the *late* transition metal in TM–TM glasses. In our study on the Ni-based glasses [26] (Ni–Y, Zr, Nb and Ni–Ti, V) we have shown that this correlation is a systematic one and points to a short-range order in the form of trigonal-prismatic units (Ni_6B, Y_6Ni respectively), connected in vertex-, edge-, and face-sharing arrangements, depending on the composition.

Here again we find that the three-peaked form of the Ni–Ni and Cu–Cu correlation functions in Y–Ni and Y–Cu is very similar to that in $Ni_{66}B_{34}$ [45], suggesting a triangular

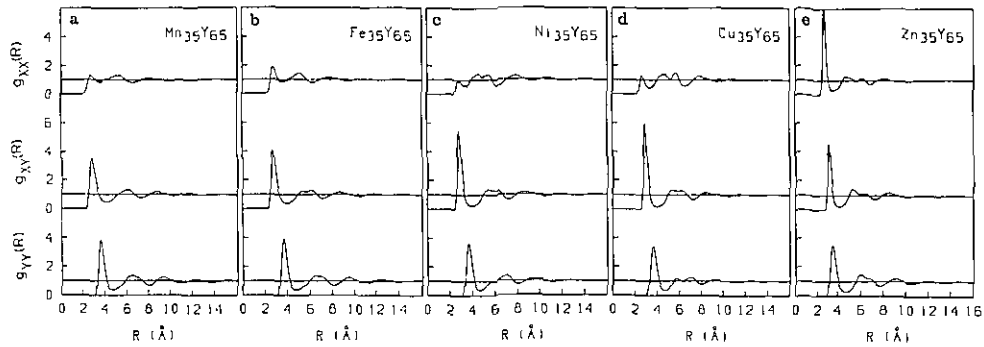

Figure 3. (a)–(e): Partial pair correlation functions for $Y_{65}X_{35}$ glasses, X = Mn, Fe, Ni, Cu, Zn.

prismatic local order. In Y–Mn, Y–Fe and also in Y–Zn the X–X correlation functions are closer to the form expected for random close packing.

3.3. Bond-angle distributions

In contrast to experiments, computer simulations allow direct access to higher-order correlation functions. The simplest three-body correlation function is the bond-angle distribution describing the distribution of the angles formed by nearest-neighbour bonds around a central atom (figure 5). There are only negligible changes in the distributions of the bond-angles around the Y atoms, but distinct variations of the bond-angles around the smaller late transition-metal atoms which show the different topology of the local atomic environment around Y and X atoms. For amorphous Y–Ni in particular, we note the similarity of the bond-angles with those in the trigonal-prismatic Y_3Ni_2 structure [47]. Y–Ni and Y–Cu are undoubtly the most strongly ordered glasses. In Y–Fe and Y–Mn the bond angles are more similar to those expected in a close-packed polytetrahedral arrangement, and this applies to Y–Zn as well. The relation between the amorphous and crystalline structures will be elaborated in more detail below.

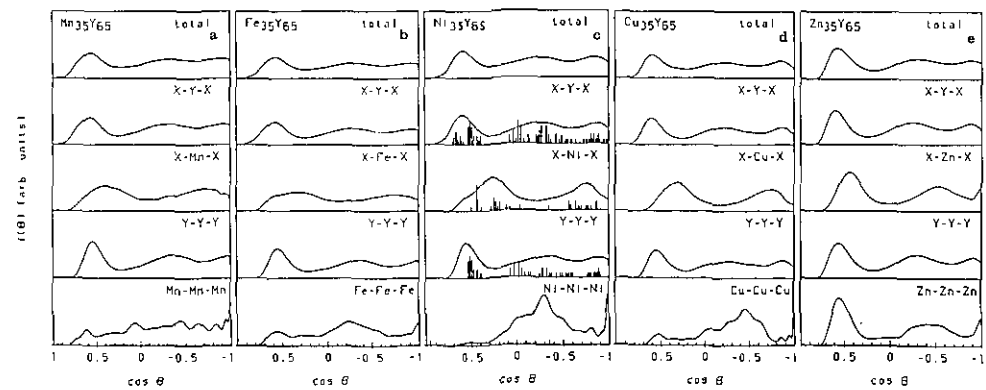

Figure 4. (a)–(e): Total, partial T–Y–T (T = X, Y), T–X–T, Y–Y–Y, and X–X–X bond-angle distributions in $Y_{65}X_{35}$, X = Mn, Fe, Ni, Cu, Zn glasses. The vertical bars indicate the bond-angles in the trigonal-prismatic crystalline Ni_3Y_2 compound (see text).

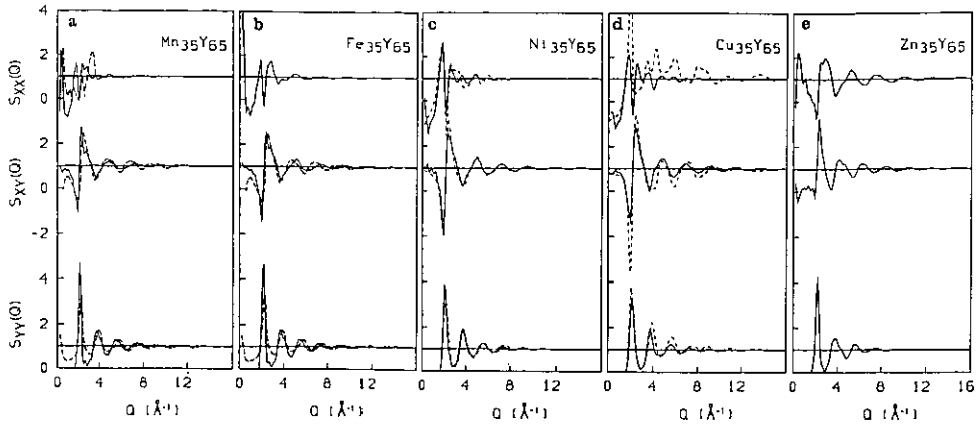

Figure 5. (a)–(e): Partial structure factors for metallic glasses $Y_{65}X_{35}$, X = Mn, Fe, Ni, Cu, Zn. The full lines show the molecular dynamics simulations, dashed lines—experimental data of Maret *et al* ([48–50]). Note that because of the isomorphic substitution assumption there is no difference in the experimental data for Y–Mn and Y–Fe.

3.4. Partial structure factors and comparison with experiment

For Y–Ni and Y–Cu attempts have been made to determine the partial structure factors by neutron-scattering experiments with isotopic substitution [48, 49]. For Fe–Mn–Y glasses an attempt has been made to determine the partial structure factors by neutron diffraction using the isomorphous substitution method between Fe and Mn atoms [50]. Judging from our pair correlation functions, the isomorphous substitution method should work quite well in this case (see figures 3(a) and (b)). In addition, a tendency to segregation has been investigated using small-angle scattering [50]. Figure 5 shows the partial structure factors for the entire series. For Y–Ni isotopic substitution leads to a good contrast between the three different interference functions, hence the resulting partial structure factors should be quite accurate. The simulations reproduce almost all the details of the very complex structure factors, a very detailed comparison between theory and experiment has already been given in [26]. For Y–Cu the situation is more difficult: as the difference in the scattering lengths of the Cu-isotopes is rather small, the coupled linear equations for the partial structure factors are rather ill-conditioned. Therefore the accuracy of the results cannot be expected to be very high. Still, the agreement between theory and experiment is quite good (figure 5(d)). The comparison suggests that the main cause of disagreement might be in a systematic error in the experimental $S_{ij}(Q)$s: for momentum transfers between about 4 Å^{-1} and 10 Å^{-1} these do not oscillate around $S_{ij} = 1$ but show systematic deviations, in a positive sense for $S_{YY}(Q)$ and $S_{CuCu}(Q)$, in a negative sense for $S_{YCu}(Q)$. A calculation of the Bhatia–Thornton structure factors shows that the error is almost entirely in the concentration-fluctuation term $S_{CC}(Q)$. This is also the only term where theory and experiment disagree, for the density-fluctuation structure factor $S_{NN}(Q)$ and for the density-concentration structure factor $S_{NC}(Q)$ the agreement is almost perfect. Eventually a reevaluation of the experimental data could eliminate the remaining uncertainty. The different character of the Fe (Mn)–Y glasses appears very clearly in the partial structure

factors. The difference is mainly in the Mn (Fe)–Mn (Fe) structure factors where the main prepeak indicative of chemical ordering is strongly reduced. The strong small-angle scattering in the Mn (Fe)–Mn (Fe) structure factor indicates a tendency to segregation by a clustering of the Mn (Fe) atoms. The tendency to segregation is clearly related to the strong covalent Mn–Mn and Fe–Fe interactions (see figure 2). The accuracy of the isomorphous substitution method is certainly lower than that of an isotopic substitution experiment, especially for the structure factor of the minority atoms (see figure 5(a) and (b)). A detailed discussion of the intensities in the small-angle scattering regime, however, would require simulations on much larger samples which are yet to be done.

3.5. Local order in amorphous and crystalline structures

In our studies of the Ni-based glasses we had shown that the local order in the glass is intimately related to the stable crystalline structures. Here we find that this applies to the Y-based glasses as well. In the Y–Mn system the stable phase with the highest content of Y is the Laves phase YMn_2. Like the two other stable phases Y_6Mn_{23} and YMn_{12}, this is a structure based on the tetrahedral close-packing principles outlined by Frank and Kasper [52]. The composition of the glass is identical with the eutectic composition, the eutectic temperature is depressed by 32% compared to the average melting temperature [53]. The Y–Fe phase diagram [54] is very similar to that of Y–Mn. The absence of Y-rich compounds correlates with the tendency to segregation in the Y–Fe and Y–Mn glasses. In the Y–Co and Y–Ni phase diagrams we find again tetrahedrally close-packed phases in the Co (Ni)-rich range (see table 3), and in addition trigonal-prismatic phases (FeB-, CrB-, cementite-type and related structures) in the Y-rich regime around the eutectic. In Y–Cu and Y–Zn the stable phase richest in Y is a CsCl-type YCu or YZn compound respectively, instead of the Laves phase we find a $CeCu_2$-type compound (dense three-dimensional packing of slightly distorted trigonal prisms), tetrahedrally close-packed phases are found only in the Cu (Zn)-rich limit. The depression of the eutectic temperature is largest in Y–Co (43.6%) and Y–Ni (39.1%) and decreases again for Y–Cu (36.5%) and Y–Zn (18.5%).

Table 3. Stable crystal structures in the Y–X (X = Mn, Fe, Ni, Cu, Zn) alloy system*.

Stoichiometry	Stable crystal structure					
X =	Mn	Fe	Co	Ni	Cu	Zn
Y_3X	—	—	*Fe_3C*	*Fe_3C*	—	—
YX	—	—	*CrB*	*FeB*	CsCl	CsCl
Y_3X_2	—	—	*Y_3Rh_2*	*Y_3Ni_2*	—	—
YX_2	**$MgCu_2$**	**$MgCu_2$**	**$MgCu_2$**	**$MgCu_2$**	*$CeCu_2$*	*$CeCu_2$*
YX_3	—	**$NbBe_3$**	**$NbBe_3$**	**$NbBe_3$**	—	**YZn_3**
YX_{5-12}	**$ThMn_{12}$**	**Th_2Ni_{17}**	**Th_2Ni_{17}**	**Th_2Ni_{17}**	**$CaCu_5$**	**$ThMn_{12}$**

Italic letters: trigonal-prismatic phases.

Boldface letters: tetrahedrally close-packed structures.

* Compiled after Villars *et al* [51].

Thus there is a clear correlation between the stability of the glass and a trigonal-prismatic local order in the crystalline and amorphous phases. Here we have shown that the origin of the trigonal-prismatic order is in the non-additive pair interactions that favour very strong, short unlike-atom bonds. This non-additivity is strongest if the atomic

d levels of the constituents are widely separated and the d bands of the pure metals show just enough overlap to cause a hybridization of the d states. The hybridization pushes the centre of gravity of the subbands even further apart (d-band shift) and emphasizes the split-band character. It is essential that pair forces are sufficient to stabilize the trigonal-prismatic local order: this type of ordering has been found not only in TM–TM (d–d) glasses, but also in TM-metalloid (p–d) glasses (Fe–B, Ni–P, Pd–Si, etc.) [55,56] and in simple-metal glasses [57,58]. This could hardly be understood if the local order were to depend on the directionality of the covalent (d–d), (p–d), and (s–p) interactions. The coexistence of trigonal-prismatic local order in crystals and glasses also requires considerable flexibility in the connectivity of the local units [55] and this can only be achieved if the bonds show no strong orientational preference.

4. Electronic structure

4.1. Supercell approach—technical details

To date, the only technique that allows for a *locally self-consistent calculation of* the electronic structure of liquid and amorphous materials is the supercell approach [57–61] applying the standard techniques of band-structure calculations for crystals to periodically repeated models of the glass. Using modern band-structure techniques such as the linear-muffin-tin-orbital (LMTO) method [62,63] supercell calculations can now be performed for models with up to a hundred atoms per cell. In our calculations we have used the scalar relativistic LMTO in the atomic sphere approximation (ASA), exchange and correlation were treated in the local-density approximation [64]. The calculations were performed for 64-atom configurations produced in a simulated MD quench (cf section 3.1). During the self-consistency loop, the calculation is done for a single special point [65] of the cubic cell ($k = (0.5,0.5,0.5)\pi/L$), for the final DOS a set of 32 k-points (the stars of the four special points $k_1 = (0.25,0.25,0.25)\pi/L$, $k_2 = (0.25,0.75,0.25)\pi/L$, $k_3 = (0.75,0.75,0.25)\pi/L$, $k_4 = (0.75,0.75,0.75)\pi/L$) has been used. The DOS is obtained from the set of discrete eigenvalues using a Gaussian broadening (the width of the Gaussian is $\sigma = 0.3$ eV). In principle, the DOS should be averaged over a set of independent configurations. However, as in our work on liquid and amorphous simple metals [57–61] and on liquid transition metals [66,67] we find only small fluctuations in the total DOS as a function of configuration. Fluctuations affect mainly the local DOS on individual sites.

4.2. Electronic density of states

Figure 6 summarizes the calculated total, site- and angular-momentum-decomposed DOS for the Y-based glasses. In all systems, the electronic DOS is characterized by a narrow band of the *late* transition metal at lower energies and a broad Y-band at higher energies. The Y bands show a quite pronounced bonding–antibonding splitting. The structure of the DOS is dominated by the d-electron contribution. In the sequence Y–X, X = Mn, Fe, Ni, Cu, Zn the d band in X is shifted to larger binding energies, in Y–Ni and Y–Cu glasses a deep DOS-minimum separates the Y- from the Ni (Cu) band. The Zn DOS in Y–Zn is very similar to that of pure Zn, with the d band barely overlapping with the bottom of the s band.

A comparison of the DOS of glassy $Y_{65}Ni_{35}$ with that calculated from crystalline Y_3Ni supports our claim of a close similarity of the local order in the amorphous and crystalline

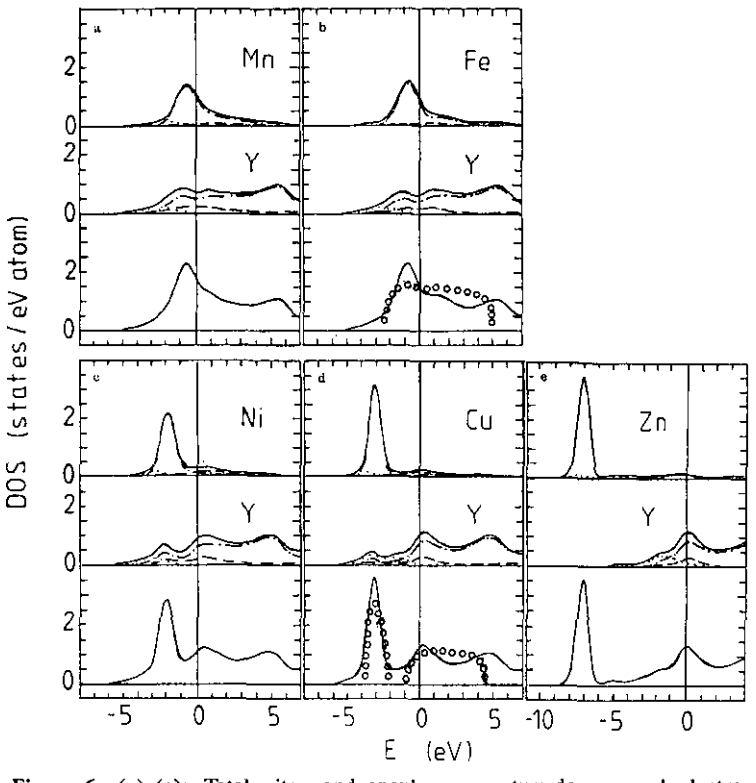

Figure 6. (a)–(e): Total, site-, and angular-momentum-decomposed electronic density of states of $Y_{65}X_{35}$ glasses, X = Mn, Fe, Ni, Cu, Zn. Full line—total DOS, dotted line—s-electron-, dashed line—p-electron-, dot-dashed line—d-electron DOS. The circles show for comparision the Bethe lattice DOS used in the calculation of the interatomic forces.

phases: the DOS of the glass is essentially a smeared-out version of the crystalline DOS (figure 7).

It is also interesting to compare the self-consistent DOS with the Bethe lattice approximation used in the calculation of the interatomic forces (see figures 1 and 6). We see that the Bethe lattice approach describes the width and the general form of the band (split versus common band) rather well, but finer details such as the bonding–antibonding splitting in the Y DOS cannot be reproduced by the Bethe lattice DOS. The main point is that the Bethe lattice approximation and the exact DOS agree at the level of detail necessary for the calculation of pair forces, although of course not at the level necessary for the interpretation of the spectroscopic information.

4.3. Photoemission intensities

A detailed comparison of the bandstructure results with photoemission experiments requires the calculation of the photoemission intensities, considering the variation of the partial photoionization cross-sections $\sigma_l(\hbar\omega, E)$ with the energy $\hbar\omega$ of the exciting photon and the binding energy E of the emitted electron. Within the LMTO-supercell technique the $\sigma_l(\hbar\omega, E)$ may be calculated from the self-consistent potentials using the following approximations [68, 69]: (a) complete neglect of wavevector conservation (note that for crystals this is appropriate only for excitation energies in the X-ray (XPS)

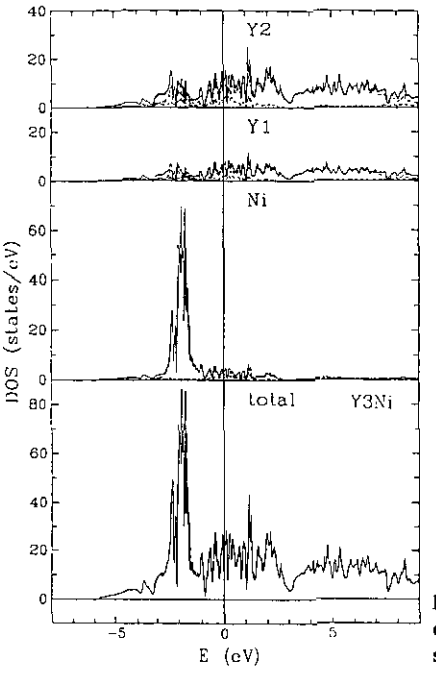

Figure 7. Total, site-, and angular-momentum-decomposed electronic density of states of crystalline Y_3Ni. For symbols see figure 6.

regime, while for glasses this holds also for the low excitation energies of the ultraviolet photoemission spectroscopy (UPS)), (b) the single-scatterer-final-state approximation, and (c) the dipole approximation to the electromagnetic field. Figure 9 shows typical XPS and UPS spectra for all Y glasses. The calculated XPS intensities have been Gaussian-broadened to account for the limited experimental resolution. The XPS spectra differ from the total DOS mainly through a small photoionization cross-section σ_d for Y d states compared to σ_d for the *late* transition metals. The low weighting factor considerably reduces the observable structure close to the Fermi level. The calculated XPS spectra may be compared with the experimental data of Tenhover *et al* [8, 9]. For the Y–X, X = Mn, Fe, Ni glasses the position, width and form of the X d band are predicted very accurately by our calculations. In Y–Zn the position of the Zn d band is shifted by about 1.6 eV to lower binding energies compared to experimental observation. A d-band shift of 0.3—0.4 eV is also found in Y–Cu glasses. A similar effect has already be found in Mg–Zn [70] and Ca–Zn [58, 71] glasses and it has been shown that it arises from the neglect of corrections for the self-energy of the d-band hole which become important for narrow bands (see also the discussion in [72] for pure crystalline Zn).

Due to the rather limited resolution and the low Y-photoionization cross-section the XPS spectra do not represent a very critical test of the electronic structure close to the Fermi level. Our results show that much better results should be obtained in a UPS study: the cross-section for Y d states is much larger and increases with decreasing binding energy. Hence the UPS spectra (figure 9(a)) show very clearly the onset of the Y band. For Y–Cu and Y–Ni experimental UPS spectra are available [73, 74]. For Y–Ni we note perfect agreement with experiment, for Y–Cu we find again a small d-band shift as in the XPS spectra. Thus the predicted split-band character of the bands is completely confirmed.

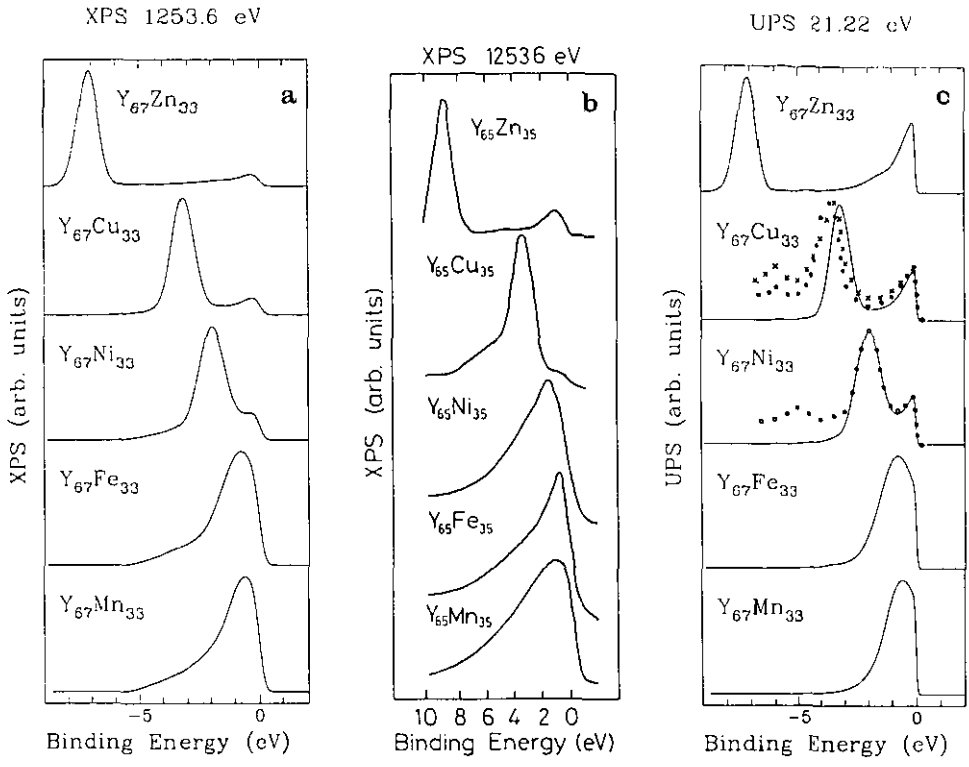

Figure 8. (a), (b) XPS spectra for Y–X glasses, X = Mn, Fe, Ni, Cu and Zn. (a) theory, (b) experiment (after Tenhover *et al* [8], [9]), photon energy $h\nu$ = 1253.6 eV. (c) UPS spectra for the Y–X glasses, X = Mn, Fe, Ni, Cu and Zn. Full line—theory (photon energy $h\nu$ = 21.2 eV), open circles—experiment (photon energy $h\nu$ = 40.8 eV, after [73]), crosses—experiment (photon energy $h\nu$ = 21.2 eV, after [74]).

5. Conclusions

Our results explain the physical origin of the strong chemical and topological short-range order effects in the atomic structure of the transition-metal glasses and their relation to the d-band shifts observed in the electronic spectra. This has been achieved by the quantum mechanical calculation of the interatomic forces using a tight-binding bond method. The bond-order for the covalent d–d bond has been calculated on a Bethe lattice as a simple, albeit realistic, reference system. We find that the Bethe lattice approximation is sufficient to reproduce the trend in the d-band complex from *a common-band to a split-band form with increasing difference in the number of d* electrons and with increasing separation of the atomic d levels. The change in the character of the d band leads to a change in the covalent bonding: in the common-band limit the bond orders are of comparable magnitude for Y–Y, Y–X, and X–X bonds and hence the interatomic forces are nearly additive; in the split-band limit the bond order is largest by far in unlike-atom bonds, leading to strongly non-additive pair forces. The non-additivity of the interatomic interaction leads to the observed short-range order in the glasses. The computer generated models of the glass have been used to calculate self-consistently the electronic DOS and the photoemission spectra. We find that (a) the calculated DOS agree reasonably well with the Bethe lattice DOS and (b) the spectra are in detailed agreement with the best available

UPS data. Point (a) is important, because it justifies the starting approximation used in the calculation of the bond-order forces. Our present results on metallic glasses of Y with other transition metals with a half- (Mn) to completely filled (Zn) d-band supplement previous work on Ni-based glasses [26] with metals with less than half-filled d bands (Y, Zr, Nb and Ti, V). Together, these results show that the structure–property relationship of the amorphous transition-metal alloys can now be investigated at a level of detail not previously possible. Ongoing work extends the present investigations to Fe-, Co-, and Ni-rich alloys showing magnetic ordering with interesting non-collinear spin structures.

Acknowledgments

This work has been supported by the Bundesministerium für Wissenschaft und Forschung within the Material Research Program (grant No 49.658/3-II/A/4/90). MT has been supported by the Bundesministerium für Wissenschaft und Forschung within the East–West Exchange Program.

We thank Dr M Maret for providing us with detailed tables of the neutron-diffraction data.

References

[1] von Minnigerode G, Samwer K, and Regenbrecht A 1987 *Amorphous and Liquid Materials* ed E Lüscher, G Fritsch and G Jacucci (Dordrecht: Nijhoft) p 435
[2] Sadoc J F and Wagner C N J 1983 *Glassy Metals II* ed H Beck and H J Güntherodt (Berlin: Springer) p 51
[3] Wagner C N J 1985 *Rapidly Quenched Metals* vol 1, ed S Steeb and H Warlimont (Amsterdam: North-Holland) p 405
[4] Suzuki K 1990 *J. Non-Cryst. Solids* **117, 118** 1
[5] Oelhafen P 1983 *Glassy Metals II* ed H Beck and H J Güntherodt (Berlin: Springer) p 283
[6] Moruzzi V L, Oelhafen P, Williams A R, Lapka R, Güntherodt H J and Kübler J 1983 *Phys. Rev.* B **27** 2049
[7] Oelhafen P, Hauser E and Güntherodt H J 1980 *Solid State Commun.* 1017
[8] Tenhover M, Lukco D and Johnson W L 1984 *J. Non-Cryst. Solids* **61, 62** 1049
[9] Tenhover M 1980 *J. Phys. F: Met. Phys.* **10** L293
[10] Connell G A N, Oh S J, Allen J and Allen R 1983 *J. Non-Cryst. Solids* **61, 62** 1061
[11] Tenhover M, Askenazi P, Lukco D and Surman D 1984 *Phys. Rev.* B **30** 618
[12] Altounian Z and Ström-Olsen J O 1983 *Phys. Rev.* B **27** 4149
[13] Trudeau M L and Cochrane R W 1990 *Phys. Rev.* B **41** 10535
[14] Ryan D H, Coey J M D, Batalla E, Altounian Z and Ström–Olsen J O 1987 *Phys. Rev.* B **35** 8630
[15] Ma H, Kunkel H P and Williams G 1991 *J. Phys.: Condens. Matter* **3** 5563
[16] Chappert J, Coey J M D, Liénard A and Rébouillat J P 1981 *J. Phys. F: Met. Phys.* **11** 2727
[17] Moorjani K and Coey J M D 1984 *Magnetic Glasses* (Amsterdam: Elsevier) section VI
[18] Coulson C A 1939 *Proc. R. Soc.* A **169** 413
[19] Pettifor D G 1989 *Phys. Rev. Lett.* **63** 2480
[20] Pettifor D G 1990 *Many-Atom Interactions in Solids* ed R M Nieminen, M J Puska and M J Manninen (Berlin: Springer) p 64
[21] Pettifor D G and Aoki M 1991 *Phil. Trans. R. Soc.* A **334** 439
[22] Carlsson A E, Fedders P A and Myles C W 1990 *Phys. Rev.* B **41** 1247
[23] Carlsson A E 1991 *Phys. Rev.* B **44** 6590
[24] Hausleitner Ch and Hafner J 1990 *J. Phys.: Condens. Matter* **2** 6651
[25] Hausleitner Ch and Hafner J 1990 *Phys. Rev.* B **42** 5863
[26] Hausleitner Ch and Hafner J 1992 *Phys. Rev.* B **45** 115; **45** 128
[27] Daw M S and Baskes M I 1984 *Phys. Rev.* B **29** 6443
[28] Jank W, Hausleitner Ch and Hafner J 1991 *Europhys. Lett.* **16** 473

[29] Hafner J, Hausleitner Ch, Jank W and Turek I 1992 *J. Non-Cryst. Solids* at press
[30] Turek I, Hausleitner Ch and Hafner J 1992 *J. Magn. Magn. Mater.* **109** L195
[31] Heine V and Weaire D 1971 *Solid State Physics* vol 24 (New York: Academic) p 247
[32] Hafner J 1987 *From Hamiltonians to Phase Diagrams* (Berlin: Springer)
[33] Ashcroft N W 1966 *Phys. Lett.* **23** 48
[34] Ichimaru S and Utsumi K 1981 *Phys. Rev.* B **24** 7385
[35] Sutton A P, Finnis M W, Pettifor D G and Ohta Y 1987 *J. Phys. C: Solid State Phys.* **21** 35
[36] Moruzzi V L 1985 *Thesis* Technische Universität Wien
[37] Hausleitner Ch, Kahl G and Hafner J 1991 *J. Phys.: Condens. Matter* **3** 1589
[38] Pettifor D G 1976 *Commun. Phys.* **1** 141
[39] Pettifor D G 1978 *J. Chem. Phys.* **69** 2930
[40] Andersen O K and Mackintosh H R 1980 *Electrons at the Fermi surface* ed M Springford (Cambridge: University Press) ch 5.3
[41] Andersen O K and Jepsen O 1977 *Physica* B **91** 317
[42] Arnold A, Mauser N and Hafner J 1989 *J. Phys.: Condens. Matter* **1** 1133
[43] Arnold A and Mauser N 1990 *Comput. Phys. Commun.* **59** 267
[44] Steeb S and Lamparter P 1985 *J. Physique Coll.* **46** C8 247
[45] Cowlam N, Gucan W, Gardener P P and Davies H A 1984 *J. Non-Cryst. Solids* **61, 62** 337
[46] Bhatia A B and Thornton D E 1970 *Phys. Rev.* B **2** 3004
[47] Dubois J M 1985 *J. Physique Coll.* **46** C8 335
[48] Maret M, Chieux P, Hicter P, Atzmon M and Johnson W L 1985 *Rapidly Quenched Metals* ed S Steeb and H Warlimont (Amsterdam: Elsevier) p 521
[49] Maret M, Chieux P, Atzmon M and Johnson W L 1987 *J. Phys. F: Met. Phys.* **17** 315
[50] Maret M, Pasturel A and Chieux P 1987 *J. Phys. F: Met. Phys.* **17** 2191;
Maret M, Simon J P and Lyon O 1989 *J. Phys.: Condens. Matter* **1** 10249
[51] Villars P, Mathis K and Hulliger F 1989 *The Structures of Binary Compounds, Cohesion and Structure* vol 2 (Amsterdam: North-Holland)
[52] Frank F C and Kasper J S 1958 *Acta Crystallogr.* **11** 184; 1959 *Acta Crystallogr.* **12** 483
[53] Hansen M and Anderko K 1958 *Constitution of Binary Alloys* 2nd edn (New York: McGraw-Hill)
[54] Moffat W G 1981 *Handbook of Binary Phase Diagrams* (Schenectady: General Electric)
[55] Gaskell P H 1983 *Glassy Metals II* ed H Beck and H J Güntherodt (Berlin: Springer) p 5
[56] Fujiwara T 1983 *Topological Disorder in Condensed Matter* ed F Yonezawa and T Ninomiya (Berlin: Springer) p 111
[57] Hafner J and Tegze M 1989 *J. Phys.: Condens. Matter* **1** 8277
[58] Tegze M and Hafner J 1989 *J. Phys.: Condens. Matter* **1** 8293
[59] Jaswal S S and Hafner J 1988 *Phys. Rev.* B **38** 7311
[60] Hafner J and Jaswal S S 1988 *Phys. Rev.* B **38** 7322
[61] Bose S K, Jaswal S S, Andersen O K and Hafner J 1988 *Phys. Rev.* B **37** 9955
[62] Andersen O K, Jepsen O and Glötzel D 1985 *Highlights of Condensed Matter Theory* ed F Bassani, I Fumi and M P Tosi (Amsterdam: North-Holland) p 113
[63] Skriver H L 1984 *The LMTO Method* (Springer, Berlin)
[64] von Barth V, Hedin L and Janak J F 1975 *Phys. Rev.* B **12** 1257
[65] Baldereschi A 1976 *Phys. Rev.* B **13** 5188
[66] Jank W, Hausleitner Ch, and Hafner J 1991 *J. Phys.: Condens. Matter* **3** 4477
[67] Hafner J and Jank W 1990 *J. Phys.: Condens. Matter* **2** SA239
[68] Jarlborg T and Nilsson P O 1979 *J. Phys. C: Solid State Phys.* **12** 265
[69] Redinger J, Marksteiner P and Weinberger P 1986 *Z. Phys.* B **63** 321
[70] Hafner J, Jaswal S S, Tegze M, Pfluigi A, Krieg J, Oelhafen P and Güntherodt H J 1988 *J. Phys. F: Met. Phys.* **18** 2583
[71] Mizutani U, Shimizu T, Fukunaga T, Koyano T, Tanaka K, Yamata M and Matsuda T 1990 *J. Phys.: Condens. Matter* **2** 7825
[72] Himpsel F J, Eastman D E, Koch E E and Williams A R 1980 *Phys. Rev.* B **32** 4604
[73] Gubler U M, Indlekofer G, Oelhafen P, Güntherodt H J and Moruzzi V L 1985 *Rapidly Quenched Metals V* ed S Steeb and H Warlimont (Amsterdam: Elsevier) p 971
[74] Frigerio J M, Martin M, Rivory J and Tran Minh Duc 1985 *Rapidly Quenched Metals V* ed S Steeb and H Warlimont (Amsterdam: Elsevier) p 1003